Coupling of the cortical hemodynamic response to cortical and thalamic neuronal activity

Anna Devor*†, Istvan Ulbert*‡§, Andrew K. Dunn*, Suresh N. Narayanan*, Stephanie R. Jones*, Mark L. Andermann*¶, David A. Boas*, and Anders M. Dale*‖

*Massachusetts General Hospital NMR Center and ¶Program in Biophysics , Harvard Medical School, Charlestown, MA 02129; ‡Institute for Psychology of the Hungarian Academy of Sciences, Budapest 1068, Hungary; and ‖Departments of Neurosciences and Radiology, University of California at San Diego, La Jolla, CA 92093

Edited by Marcus E. Raichle, Washington University School of Medicine, St. Louis, MO, and approved January 25, 2005 (received for review October 20, 2004)

Accurate interpretation of functional MRI (fMRI) signals requires knowledge of the relationship between the hemodynamic response and the neuronal activity that underlies it. Here we address the question of coupling between pre- and postsynaptic neuronal activity and the hemodynamic response in rodent somatosensory (Barrel) cortex in response to single-whisker deflection. Using full-field multiwavelength optical imaging of hemoglobin oxygenation and electrophysiological recordings of spiking activity and local field potentials, we demonstrate that a point hemodynamic measure is influenced by neuronal activity across multiple cortical columns. We demonstrate that the hemodynamic response is a spatiotemporal convolution of the neuronal activation. Therefore, positive hemodynamic response in one cortical column might be explained by neuronal activity not only in that column but also in the neighboring columns. Thus, attempts at characterizing the neurovascular relationship based on point measurements of electrophysiology and hemodynamics may yield inconsistent results, depending on the spatial extent of neuronal activation. The finding that the hemodynamic signal observed at a given location is a function of electrophysiological activity over a broad spatial region helps explain a previously observed increase of local vascular response beyond the saturation of local neuronal activity. We also demonstrate that the oxy- and total-hemoglobin hemodynamic responses can be well approximated by space–time separable functions with an antagonistic center-surround spatial pattern extending over several millimeters. The surround ''negative'' hemodynamic activity did not correspond to observable changes in neuronal activity. The complex spatial integration of the hemodynamic response should be considered when interpreting fMRI data.

Barrel cortex | blood oxygenation | intrinsic signals | optical imaging

The advent of noninvasive imaging methods such as functional MRI (fMRI) has made it possible to obtain spatial maps of hemodynamic ''activation'' in the human brain under a variety of conditions (1, 2). However, the indirect and poorly understood nature of the coupling between these hemodynamic signals and the underlying neuronal activity has greatly limited the interpretability of neuroimaging results. Recently, several groups have attempted to characterize this coupling in the form of a linear or nonlinear neurovascular ''transfer function'' (3–8). In principle, if such a function could be defined, it would provide a basis for inferring time-averaged local neuronal activity based on hemodynamic measurements. Furthermore, it would permit more accurate integration of hemodynamic imaging methods with noninvasive electrophysiological recordings such as electroencephalography and magnetoencephalography (9, 10).

In a previous publication (3), using simultaneous spectroscopic optical imaging and electrophysiological measurements in rodent somatosensory cortex during brief and spatially localized stimuli, we found a strongly nonlinear relationship between point hemodynamic and neuronal signals. Specifically, our results showed that with an increase in stimulus amplitude, the hemodynamic response recorded from the region of interest (ROI) surrounding the recording electrode increased beyond the saturation of electrical activity as reflected in multiple unit activity (MUA) and local field potential (LFP) measurements. Subsequently, other groups have produced consistent results in the same system by using both tactile and electrical stimuli (4, 8).

This apparent mismatch between neuronal and hemodynamic behavior may result from neuronal processes, such as a neurotransmitter release from presynaptic thalamic terminals, undetected by the electrophysiological recording methods used (11–13). Here we present data showing that the hemodynamic response within a cortical column (a principal barrel in Barrel cortex) increases beyond saturation of the thalamic input to the same column. It is therefore likely that the hemodynamic response measured in the principal barrel column is driven at least in part by neuronal activity outside the column. Indeed, the neuronal response in neighboring barrels was observed to increase throughout the stimulus range, thus providing a potential explanation for monotonically increasing hemodynamic response within a principal barrel beyond saturation of the local electrophysiological response.

Methods

The methods are described in detail in ref. 3.

Animal Preparation. Male Sprague–Dawley rats ($n = 17$, 250–350 g, Taconic Farms) were used. All experimental procedures were approved by the Massachusetts General Hospital Subcommittee on Research Animal Care. Rats were initially anesthetized with 1.5% halothane and ventilated with ≈1% halothane in a mixture of air and oxygen. Halothane was discontinued, and anesthesia was maintained with a 50-mg·kg^{-1} i.v. bolus of α-chloralose followed by continuous i.v. infusion at 40 mg·kg^{-1}·h^{-1}. Heart rate, blood pressure, blood gas, and body temperature were monitored.

An area of skull overlying the primary somatosensory cortex was exposed and then thinned until soft and transparent (≈100 μm). A well of petroleum jelly was built and filled with mineral oil (Sigma). A small hole was made in the thinned skull over the center of a barrel, as determined by optical imaging, and the recording electrode was introduced through the dura mater. For

This paper was submitted directly (Track II) to the PNAS office.

Freely available online through the PNAS open access option.

Abbreviations: MUA, multiple unit activity; LFP, local field potential; ROI, region of interest; fMRI, functional MRI; Hb, deoxyhemoglobin; HbO, oxyhemoglobin; HbT, total hemoglobin; VPM, ventral posteriomedial thalamic nucleus; POm, medial division of the posterior thalamic nucleus.

†To whom correspondence should be addressed. E-mail: adevor@nmr.mgh.harvard.edu.

§I.U. recently founded and is the majority owner of Neurotrack, a company that develops and markets laminar electrophysiology equipment for animal research.

www.pnas.org/cgi/doi/10.1073/pnas.0407789102

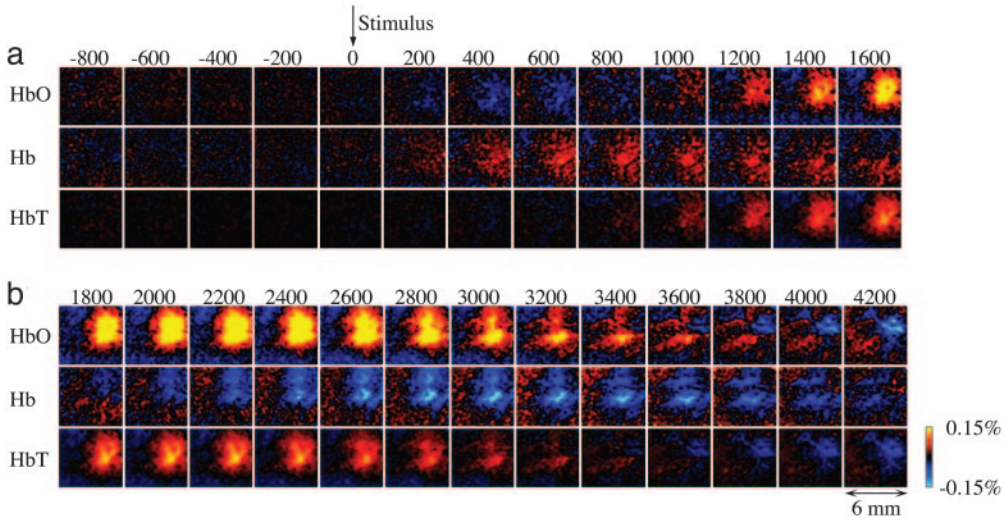

Fig. 1. Spatiotemporal evolution of the hemodynamic reponse. (*a*) Full-field time series of HbO, Hb, and HbT signals (an average of the six strongest stimulus amplitudes) were calculated from six wavelength data. Each image represents an individual frame (average of ≈1,400 trials). Time between consecutive images is 200 msec. (*b*) A continuation of the time series shown in *a*. The signal for Hb and HbO is expressed in percent change relative to its own baseline concentration (40 and 60 μM, respectively, were assumed for all animals). HbT was calculated as a sum of Hb and HbO.

recordings involving laminar probes, the thinned skull and dura mater were removed.

Spectroscopic Optical Imaging. To illuminate the cortex, light from a mercury xenon arc lamp was directed through a six-position rotating filter wheel (560, 570, 580, 590, 600, and 610 nm) coupled to a 12-mm fiber bundle. Images of a 4.5- to 6-mm^2 area were acquired by a cooled 12-bit charge-coupled device camera (Coolsnap, Photometrics, Tucson, AZ). Image acquisitions were triggered at ≈15 Hz by individual filters in the filter wheel passing through an optic sensor (14). The spectral data were converted to percent change maps for deoxyhemoglobin (Hb), oxyhemoglobin (HbO), and total hemoglobin (HbT) by using the modified Beer–Lambert law (14). Differential pathlength correction was applied to adjust for the differential optical pathlength through the tissue at different wavelengths. The point-spread function for the optical signal was estimated as 100 μm in the lateral plane at a depth of 400 μm from the cortical surface.

Electrophysiological Recordings. Electrophysiological recordings were performed by using either single metal microelectrodes [FHC (Bowdoinham, ME), 5–7 MΩ] or linear array multielectrodes with 24 contacts spaced at 100 μm (15). Layer IV was identified by depth and a selective response to the principal whisker. By using array microelectrodes, the depth was estimated based on a contact number when contact no. 1 was positioned at the cortical surface by using visual control. A contact with the strongest selectivity was identified by listening to an audio monitor while stimulating different whiskers. The signals were amplified and filtered between 500 and 5,000 Hz to record MUA and between 0.1 and 500 Hz to record LFP. The MUA signals were rectified on the time axis before averaging. Averaged LFP curves were rectified on the time axis before integration. In cortex, the microelectrodes were positioned in lower layer II/III (400–500 μm). The ventral posteriomedial thalamic nucleus (VPM) and the medial division of the posterior thalamic nucleus (POm) were targeted by using stereotactic coordinates (VPM, AP −3.6 to −3.0, ML 2.0 to 3.5, and DV 5.0 to 7.0; POm, AP −4.3 to −3.5, ML 1.5 to 2.5, and DV 5.0 to 6.5).

Stimulation Paradigm. Single whiskers were deflected upward by a wire loop coupled to a computer controlled piezoelectric stimulator. We used a fast randomized event-related stimulus presentation paradigm analogous to that used in event-related fMRI studies. The stimulus sequence was optimized for event-related response estimation efficiency by using the approach described by Dale (16). The stimulation paradigm consisted of single deflections of varying amplitude with an interstimulus interval of 1 sec. We used 27 stimulus amplitudes. Intervening amplitudes were spaced with equal increments on a linear scale. The stimulus angular velocity increased from 203° per sec (vertical displacement of 240 μm, amplitude 1) to 969° per sec (vertical displacement of 1,200 μm, amplitude 27). For each stimulus condition, we averaged 240 trials for each animal.

Results

The Barrel cortex in the rat is well suited for studying localized cortical activations due to precise mapping of each one of the large facial vibrissae (whiskers) onto a specific cortical area, called a barrel (17). In agreement with previous reports, tactile stimulation of a single facial whisker produced spatially localized optical signals centered on the principal barrel and extending well beyond one cortical column (18). Fig. 1 shows activation maps of HbO, Hb, and HbT as a function of time after deflection of a single whisker. These maps were calculated by using full-field time-resolved spectral optical measurements obtained with a rotating filter wheel (see *Methods*). In agreement with our previous report (3), an initial increase ("initial dip") in Hb was accompanied by an initial decrease in HbO, both preceding an increase in HbT (Fig. 1; see also Fig. 7, which is published as supporting information on the PNAS web site). These early changes may correspond to a local increase in oxygen consumption preceding an increase in blood flow (19, 20). A subsequent increase in HbT (reflecting an increase in blood volume under the assumption of constant hematocrit) was accompanied by a reversal of sign in both Hb and HbO signals, presumably corresponding to washout of Hb by increased blood flow (21). The hemodynamic signals always exhibited an antagonistic center-surround spatial pattern. The increase in HbO and HbT centered on the principal barrel was always accompanied by corresponding decreases in the surround. Similarly, a decrease in

NEUROSCIENCE

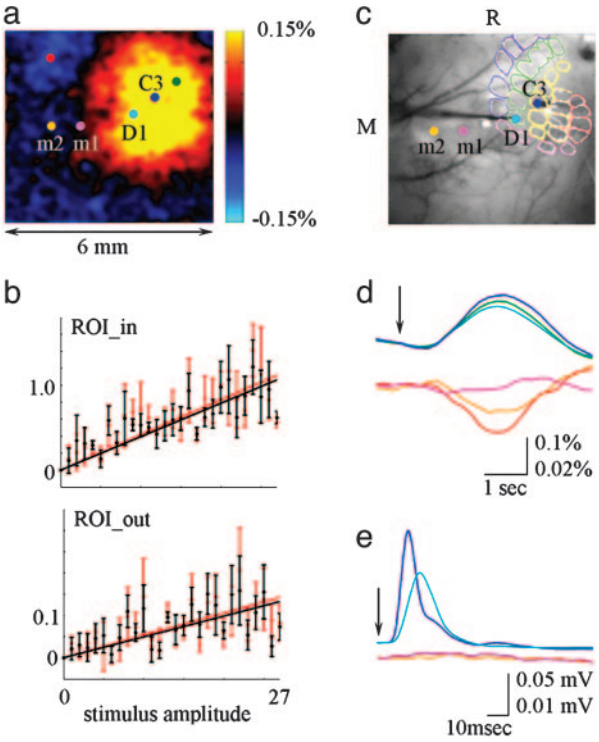

Fig. 2. The hemodynamic response has an antagonistic center-surround spatial pattern. (*a*) An image of HbO at the peak of the response. (*b*) Integral HbO (red) and HbT (black) responses as a function of stimulus intensity in the center (principal barrel, ROI_in) and surround (>3 mm away from the recording electrode, ROI_out). Data from five animals were averaged, and all amplitudes are shown. The error bars reflect the intersubject standard error. The center and surround response amplitudes in every animal were normalized to the maximal response amplitude in the center ROI for that animal before averaging the data across animals. Note that the magnitude of the negative surround response is on average ≈10% of that in the center. (*c*) The locations of electrophysiological recordings are superimposed on the image of the vasculature corresponding to the functional map in *a*. Recordings from locations m1 and m2 were performed after recordings from C3 and D1 barrels (the electrodes are visible on the image). The indicated approximate location of the Barrel field was determined by fitting the position, size, and orientation of a typical histology sample based on the locations of two identified barrel columns (C3 and D1). (*d*) Time courses of HbT response averaged from 300 × 300 μm ROIs around recording electrodes. The locations are color coded in *a* and *c*. (*e*) MUA recorded from the locations marked in *c*. Responses to seven largest stimulus amplitudes are averaged in *d* and *e*. The vertical scales for the top and bottom plots in *d* and *e* differ by factor of 5. The arrow denotes stimulus delivery.

Hb in the center was always accompanied by an increase in the surround.

A comparison of the center-surround pattern of the HbO response at the peak of activation (Fig. 2*a*) to an estimated size of the Barrel cortex (Fig. 2*c*) shows that the center "positive" activity covers approximately the entire Barrel cortex, whereas the surround "negativity" is present outside Barrel cortex, and even outside the primary somatosensory cortex (22). The hemodynamic response as a function of stimulus intensity was investigated in the regions corresponding to the principal barrel and the surround "negativity" (Fig. 2). The first ROI was defined as a 300 × 300-μm area around the electrode used to record spiking (MUA) and synaptic (LFP) neuronal activity from the principal barrel. Taking into account the distance between the adjacent barrels of ≈500 μm (23), this ROI reflected the hemodynamic response in the principal barrel column. The second ROI was defined as all pixels at least 3 mm away from the recording electrode, reflecting the region of

Table 1. Percent variance explained by the first principal component analysis for HbO, Hb, and HbT signals

Case ID	HbO	Hb	HbT
72204	94.00	76.00	95.00
72604	79.00	42.00	85.00
60704	70.00	36.00	82.00
60104	68.00	35.00	76.00
60204	85.00	58.00	87.00

Each row represents one case (one animal). ID, identification.

surround negativity well outside the Barrel cortex. An amplitude of the hemodynamic response increased with an increase in stimulus intensity in both the center and surround ROIs (Fig. 2*b*), with a surround amplitude in average ≈10% of that in the center. A comparison of hemodynamic responses averaged from 300 × 300-μm ROIs around recording electrodes with electrophysiological recordings showed no change in neuronal activity in the surround region (Fig. 2 *d* and *e*; see also Fig. 8, which is published as supporting information on the PNAS web site). Thus, the surround negative response did not correspond to local neuronal inhibition, as measured by our methods. The spatiotemporal pattern of the hemodynamic activity including the biphasic spatial pattern is also evident in our previous data using a different anesthesia agent, urethane, which indicates a conservation of the phenomenon across anesthesia conditions and rules out a possibility that the center-surround pattern is an artifact of α-chloralose (3).

Principal component analysis revealed one dominant component explaining most of the variance for the HbO and HbT spatiotemporal observations and, to a lesser extent, Hb (Table 1; see also Fig. 9, which is published as supporting information on the PNAS web site). The more complex behavior of Hb may reflect a combination of competing effects of oxygen consumption, blood volume changes, and washout process at different timescales. The stimulus dependence of the surround negativity (Fig. 2*b*) and the results of principal component analysis indicate space–time separability of HbO and HbT hemodynamic activation, where the response at every time point and stimulus amplitude represents a scaling version of a fixed center-surround spatial pattern.

Consistent with our previous results (3), the hemodynamic response within the principal barrel continued to increase beyond saturation of MUA and LFP recorded from the same barrel (Fig. 3; see also Fig. 10, which is published as supporting information on the PNAS web site). The hemodynamic response in the principal barrel increased monotonically throughout the stimulus range. An approximately linear relationship was ob-

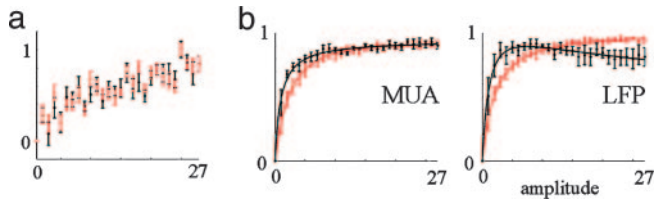

Fig. 3. The local hemodynamic response increases beyond saturation of local neuronal activity. (*a*) Integral HbO (red) and HbT (black) responses averaged from 300 × 300 μm ROI around the electrode recording from the principal barrel as a function of stimulus intensity. Data from eight animals were averaged, and all amplitudes are shown. The error bars reflect the intersubject standard error. (*b*) MUA (*Left*), LFP (*Right*) peak (red), and integral (black) responses as a function of stimulus amplitude. The data were averaged across the same subjects as in *a*. The curves were fitted by using the function $ax/(1-bx)^c$.

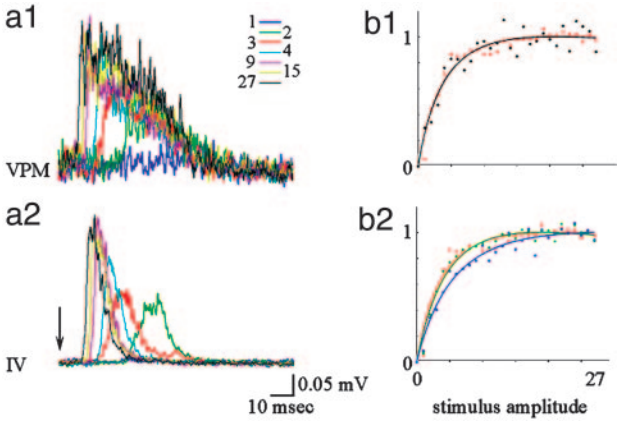

Fig. 4. Thalamic VPM and cortical responses saturate with an increase in stimulus intensity. (*a1*) MUA activity was recorded simultaneously in thalamus (VPM) by using a single metal electrode and in the cortex by using a laminar electrode array. Responses for different stimulus amplitudes (*Inset*) are superimposed for VPM (*Upper*) and cortical layer IV (*a2*). An input impedance of recording electrodes, 7 MΩ in the VPM and 0.2 MΩ in the cortex, explains differences in signal-to-noise ratio. (*b1*) VPM (black) and cortical layer IV (red) peak response as a function of stimulus intensity. The curves were fitted by using the function $ax/(1-bx)^c$. (*b2*) Granule (layer IV, red), supragranule (blue) and infragranule (green) peak responses as a function of stimulus amplitude.

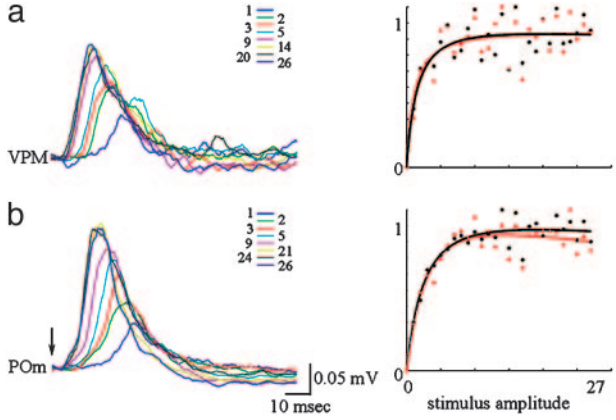

Fig. 5. Neither lemniscal nor paralemniscal inputs increase beyond saturation of the postsynaptic activity. (*a*) MUA activity was simultaneously recorded from VMP and POm by using two laminar electrode arrays. Responses for different stimulus amplitudes (*Inset*) are superimposed for VPM (*a*) and POm (*b*). The peak (black) and integral (red) response as a function of stimulus intensity was fitted by using the function $ax/(1-bx)^c$.

served between the hemodynamic response, measured as the integral under the timecourse curve, and the stimulus amplitude (Fig. 3*a*). Note that the conserved spatiotemporal pattern of the hemodynamic response for HbO and HbT (Fig. 9) implies that a time course averaged from any other ROI will behave as a scaled version of that from the principal barrel ROI. In contrast to the hemodynamic response, spiking and synaptic neuronal activity recorded from the principal barrel as MUA and LFP, respectively, exhibited saturation with an increase in stimulus intensity. LFP measures a weighted sum of transmembrane currents due to synaptic and dendritic activity (24, 25), whereas MUA measures population spiking activity (26, 27). We estimated a total evoked neuronal activity by using the integral under the curve and peak values for MUA and LFP. All measures showed pronounced saturation with an increase in stimulus intensity (Fig. 3*b*).

Sensory inputs from the whisker pad reach Barrel cortex via two parallel pathways: lemniscal (via the VPM) and paralemniscal (via the medial division of the posterior thalamic nucleus, POm) (28–30). In the VPM, each facial vibrissa is mapped onto a cluster of cells (a barreloid) that sends its output to the corresponding cortical barrel (31). The POm has more diffuse maps, longer latencies, and a strong dependence on cortical feedback (32). To test whether the apparent mismatch between neuronal and hemodynamic behavior results from a presynaptic (thalamic) process, we performed simultaneous measurements from corresponding locations in the cortex and thalamus. Simultaneous measurements from the corresponding barreloid in the VPM showed that the input cortical layer (layer IV) followed closely the thalamic input. Fig. 4 shows the MUA response in thalamus (Fig. 4*a1*) and cortical input layer IV (Fig. 4*a2*). Fig. 4*b1* shows an increase in response in thalamus (black) and cortical layer IV (red) as a function of stimulus intensity. The same function $[ax/(1-bx)^c]$ fits well both cortical and thalamic VPM spiking activity. Therefore, the saturation of the MUA in layer IV of the cortex is fully explained by saturation in the input from the VPM. Note that the similarity in the cortical and thalamic responses under our stimulus conditions should not be taken as a general case. Thalamocortical response transformation can be readily demonstrated by using other stimulus paradigms such as whisker deflections with different rise time (33), prolong "ramp-and-hold" trapezoids (34) or repetitive stimulation (28).

The results of simultaneous laminar recordings of MUA from VPM and POm are shown in Fig. 5. In agreement with previous reports (32), POm responses peaked later in time (Fig. 5*b*) and were distributed through a number of recording electrodes indicating diffuse mapping (data not shown). Recordings from the electrode with the shortest delay are shown in Fig. 5. Both VPM and POm MUA responses, measured either as peak values or an integral under the curve (Fig. 5 *Right*; see also Fig. 11, which is published as supporting information on the PNAS web site) saturated with an increasing stimulus intensity.

Because the hemodynamic response recorded from the principal barrel increases beyond saturation of both the pre- and postsynaptic activity localized to the same barrel, processes outside the principal barrel must contribute. To investigate the MUA and LFP behavior in neighboring cortical columns, we performed simultaneous recordings from the principal barrel and a neighbor barrel (Fig. 6; see also Figs. 12 and 13, which are published as supporting information on the PNAS web site). In agreement with previous reports, MUA and LFP activity in the neighbor barrel had a smaller amplitude and a slower rise (Fig. 6 *a* and *b*) (35). Fig. 6*d* shows locations of the electrode recordings from columns corresponding to δ, D2, and D3 whiskers. The fastest saturation of the neuronal activity was present in the principal barrel column δ (Fig. 6*c*, red), followed by D2 column located two columns away (Fig. 6*c*, blue). In the D3 column, located three columns away from the principal barrel, neuronal activity increased close to linear throughout the stimulus range (Fig. 6*c*, green).

Discussion

Our results show that the neurovascular transfer function is nonlocal, i.e., the hemodynamic signal observed at a given location is a function of electrophysiological activity over a broad spatial region. Thus, attempts at characterizing this function based on point measurements of electrophysiology and hemodynamics may yield inconsistent results, depending on the spatial extent of neuronal activation. This may explain some of the apparent discrepancies in the neurovascular relationship between the results reported while using varying stimulus frequencies vs. varying stimulus amplitudes in rat Barrel cortex (5–8). Note that the nonlocal nature of the hemodynamic point spread

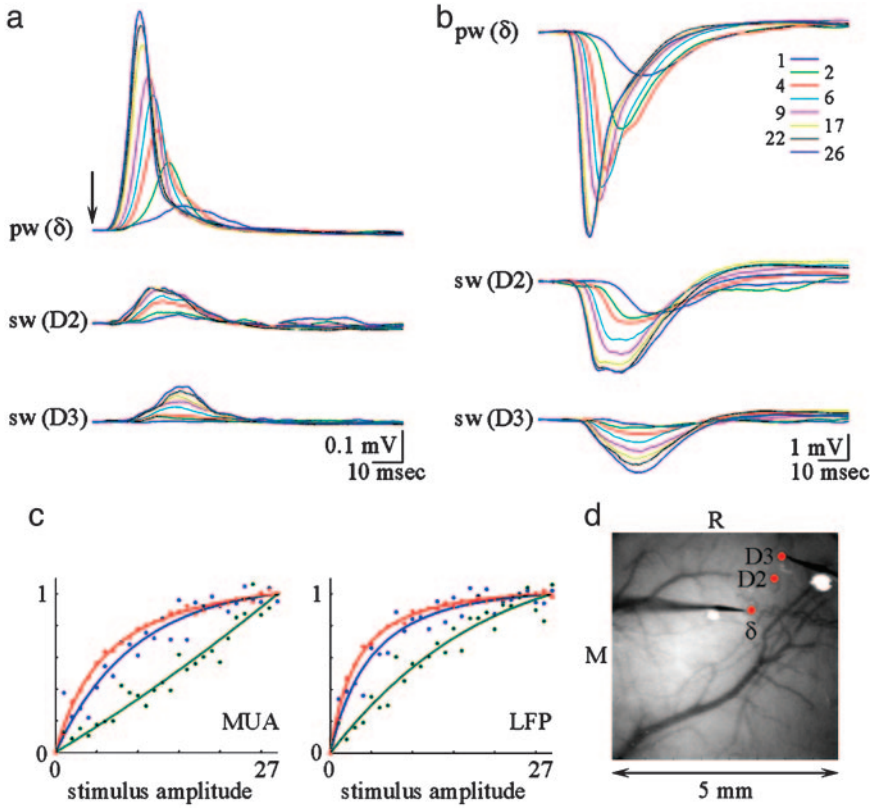

Fig. 6. Neuronal activity in neighboring cortical columns increases throughout the stimulus range. MUA (*a*) and LFP (*b*) responses are plotted for the principal barrel (δ) and two neighboring barrels (D2 and D3). Responses to different amplitudes are superimposed (*Inset*). The arrow denotes stimulus delivery. (*c*) MUA (*Left*) and LFP (*Right*) peak responses as a function of stimulus amplitude. The curves were fitted by using the function $ax/(1-bx)^c$. (*d*) Locations of electrophysiological recordings are superimposed on the image of the vasculature. Recordings from barrel columns δ and D3 (the electrodes are visible on the image) were performed after recordings from δ and D2 barrels.

does not necessarily preclude accurate localization of individual columns based on the center of mass of the hemodynamic response, e.g., due to deflection of individual whiskers (36), or by subtracting one stimulus condition from another (37, 38). However, it does limit the achievable resolution in terms of two-point separation (39).

The relatively large spatial extent of the hemodynamic response is in agreement with previous optical imaging studies (18). Although spiking activity after a deflection of a single whisker is largely restricted to a small number of neighboring barrel columns (35), voltage-sensitive dye imaging shows that neuronal activity after a brief deflection of a single whisker spreads from the principal barrel column to cover a large part of the Barrel cortex (23). Both extensive lateral cortico-cortical connections (35, 40) and diffuse nonlemniscal inputs (32) might contribute to this significant lateral spread of neuronal activity. Because voltage-sensitive dye measurements are sensitive to subthreshold neuronal activity (41, 42), this observation also advocates a significant contribution of subthreshold synaptic activity to hemodynamic signals.

In addition, a number of phenomena other than sub- or suprathreshold local neuronal activity have been demonstrated to contribute to increase the spatial spread of the hemodynamic response. Among them are the diffusion of vasodilator substances such as NO from the active locus to nearby vessels (43, 44) after an increase in intracellular calcium (45), conducted upstream and downstream vasodilatation (46, 47), and innervation of cortical microvessels by cholinergic fibers originating from basal forebrain and/or 5-HT fibers originating from raphe nuclei. Both cholinergic and 5-HT inputs have been shown to induce significant increases in cortical perfusion upon stimulation (48, 49).

The antagonistic hemodynamic changes observed in the surround, in the absence of corresponding neuronal deactivation, strongly suggest that the neurovascular transfer function has a center-surround structure. Our measurement of MUA and LFP in the surround area of hemodynamic activation failed to reveal any neuronal correlate such as surround neuronal inhibition. However, a possibility exists that a decrease in pyramidal neuron activity in the surround area is exactly balanced by an increase in inhibitory interneuron activity, resulting in unchanged MUA. It is also possible that dendritic activity of inhibitory interneurons would not show up on our LFP recordings due to their closed-field configuration. Although we cannot rule out this hypothesis based on the current data, we find it unlikely taking into account the spatial extent of the negative hemodynamic activation. In the present experiment, this negative surround extends beyond the Barrel cortex and even beyond the somatosensory complex. To our knowledge, there have been no reports of electrophysiological response outside of the Barrel cortex to brief single-whisker deflection stimuli as used in this study. Negative surround activation has also previously been reported by using blood oxygen level-dependent fMRI in high-order visual areas where neuronal activation rather than deactivation is expected to occur under the stimulus conditions used (50).

The stimulus amplitude dependence of the surround negativity, along with the results of principal component analysis, suggests a spatiotemporal separability of the neurovascular transfer function for HbO and HbT. The corresponding analyses for Hb, on the other hand, reveal a more complex pattern of

results. Specifically, the spatial pattern of the Hb response varies as a function of poststimulus latency. A detailed analysis of spatiotemporal dynamics of Hb could provide more insight into the competing effects of flow, volume, and oxygen consumption ($CMRO_2$) changes in blood oxygen level-dependent fMRI signal, because this method is primarily sensitive to changes in Hb (51).

A precise characterization of the neurovascular transfer function will require full-field imaging of both electrophysiological and hemodynamic parameters under different stimulus conditions, where the location and extent of neuronal activation are systematically varied. This could be accomplished by combining simultaneous spectroscopic and voltage-sensitive dye imaging (52) during stimulation of different whiskers at varying frequencies, which is known to modulate the lateral spread of neuronal activity (53) and the hemodynamic response (54, 55).

The complex spatial and temporal structure of the neurovascular transfer function evident in the present study has important implications for the proper interpretation of fMRI results and for the integration of different imaging modalities (10). In particular, the spatial extent, center-surround organization, and nonlinear gain of the neurovascular coupling have to be considered to draw valid inferences about neuronal activity from hemodynamic measures.

This work was supported by National Institutes of Health Grants R01 EB00790, P41 RR14075, and NS44623 and by the Mental Illness and Neuroscience Discovery (MIND) Institute.

1. Kwong, K. K., Belliveau, J. W., Chesler, D. A., Goldberg, I. E., Weisskoff, R. M., Poncelet, B. P., Kennedy, D. N., Hoppel, B. E., Cohen, M. S., Turner, R., *et al*. (1992) *Proc. Natl. Acad. Sci. USA* **89,** 5675–5679.
2. Belliveau, J. W., Kennedy, D. N., Jr., McKinstry, R. C., Buchbinder, B. R., Weisskoff, R. M., Cohen, M. S., Vevea, J. M., Brady, T. J. & Rosen, B. R. (1991) *Science* **254,** 716–719.
3. Devor, A., Dunn, A. K., Andermann, M. L., Ulbert, I., Boas, D. A. & Dale, A. M. (2003) *Neuron* **39,** 353–359.
4. Jones, M., Hewson-Stoate, N., Martindale, J., Redgrave, P. & Mayhew, J. (2004) *NeuroImage* **22,** 956–965.
5. Nemoto, M., Sheth, S., Guiou, M., Pouratian, N., Chen, J. W. & Toga, A. W. (2004) *J. Neurosci.* **24,** 3850–3861.
6. Martindale, J., Mayhew, J., Berwick, J., Jones, M., Martin, C., Johnston, D., Redgrave, P. & Zheng, Y. (2003) *J. Cereb. Blood Flow Metab.* **23,** 546–555.
7. Sheth, S., Nemoto, M., Guiou, M., Walker, M., Pouratian, N. & Toga, A. W. (2003) *NeuroImage* **19,** 884–894.
8. Sheth, S. A., Nemoto, M., Guiou, M., Walker, M., Pouratian, N. & Toga, A. W. (2004) *Neuron* **42,** 347–355.
9. Dale, A. M., Liu, A. K., Fischl, B. R., Buckner, R. L., Belliveau, J. W., Lewine, J. D. & Halgren, E. (2000) *Neuron* **26,** 55–67.
10. Dale, A. M. & Halgren, E. (2001) *Curr. Opin. Neurobiol.* **11,** 202–208.
11. Frerking, M. & Wilson, M. (1996) *Curr. Opin. Neurobiol.* **6,** 395–403.
12. Lauritzen, M. (2001) *J. Cereb. Blood Flow Metab.* **21,** 1367–1383.
13. Tang, C. M., Margulis, M., Shi, Q. Y. & Fielding, A. (1994) *Neuron* **13,** 1385–1393.
14. Dunn, A. K., Devor, A., Bolay, H., Andermann, M. L., Moskowitz, M. A., Dale, A. M. & Boas, D. A. (2003) *Opt. Lett.* **28,** 28–30.
15. Ulbert, I., Halgren, E., Heit, G. & Karmos, G. (2001) *J. Neurosci. Methods* **106,** 69–79.
16. Dale, A. M. (1999) *Hum. Brain Mapp.* **8,** 109–114.
17. Woolsey, T. A. & Van der Loos, H. (1970) *Brain Res.* **17,** 205–242.
18. Masino, S. A., Kwon, M. C., Dory, Y. & Frostig, R. D. (1993) *Proc. Natl. Acad. Sci. USA* **90,** 9998–10002.
19. Shtoyerman, E., Arieli, A., Slovin, H., Vanzetta, I. & Grinvald, A. (2000) *J. Neurosci.* **20,** 8111–8121.
20. Vanzetta, I. & Grinvald, A. (2001) *NeuroImage* **13,** 959–967.
21. Fox, P. T. & Raichle, M. E. (1986) *Proc. Natl. Acad. Sci. USA* **83,** 1140–1144.
22. Welker, C. (1971) *Brain Res.* **26,** 259–275.
23. Petersen, C. C., Grinvald, A. & Sakmann, B. (2003) *J. Neurosci.* **23,** 1298–1309.
24. Eccles, J. C. (1951) *Electroencephalogr. Clin. Neurophysiol.* **3,** 449–464.
25. Plonsey, R. & Heppner, D. B. (1967) *Bull. Math. Biophys.* **29,** 657–664.
26. Legatt, A. D., Arezzo, J. & Vaughan, H. G., Jr. (1980) *J. Neurosci. Methods* **2,** 203–217.
27. Mitzdorf, U. (1987) *Int. J. Neurosci.* **33,** 33–59.
28. Ahissar, E., Sosnik, R. & Haidarliu, S. (2000) *Nature* **406,** 302–306.
29. Koralek, K. A., Jensen, K. F. & Killackey, H. P. (1988) *Brain Res.* **463,** 346–351.
30. Lu, S. M. & Lin, R. C. (1993) *Somatosens. Motil. Res.* **10,** 1–16.
31. Van der Loos, H. (1976) *Neurosci. Lett.* **2,** 1–6.
32. Diamond, M. E., Armstrong-James, M. & Ebner, F. F. (1992) *J. Comp. Neurol.* **318,** 462–476.
33. Pinto, D. J., Brumberg, J. C. & Simons, D. J. (2000) *J. Neurophysiol.* **83,** 1158–1166.
34. Simons, D. J. & Carvell, G. E. (1989) *J. Neurophysiol.* **61,** 311–330.
35. Brecht, M., Roth, A. & Sakmann, B. (2003) *J. Physiol.* **553,** 243–265.
36. Sheth, S. A., Nemoto, M., Guiou, M., Walker, M., Pouratian, N., Hageman, N. & Toga, A. W. (2004) *J. Neurosci.* **24,** 634–641.
37. Harrison, R. V., Harel, N., Kakigi, A., Raveh, E. & Mount, R. J. (1998) *Audiol. Neurootol.* **3,** 214–223.
38. Malonek, D. & Grinvald, A. (1996) *Science* **272,** 551–554.
39. Strutt, J. W., III Lord Rayleigh (1879) *Philos. Mag.* **VIII**.
40. Manns, I. D., Sakmann, B. & Brecht, M. (2004) *J. Physiol.* **556,** 601–622.
41. Ebner, T. J. & Chen, G. (1995) *Prog. Neurobiol.* **46,** 463–506.
42. Grinvald, A., Frostig, R. D., Lieke, E. & Hildesheim, R. (1988) *Physiol. Rev.* **68,** 1285–1366.
43. Gulbenkian, S., Uddman, R. & Edvinsson, L. (2001) *Peptides* **22,** 995–1007.
44. Snyder, S. H. & Bredt, D. S. (1991) *Trends Pharmacol. Sci.* **12,** 125–128.
45. Lauritzen, M. (2005) *Nat. Rev. Neurosci.* **6,** 77–85.
46. Cox, S. B., Woolsey, T. A. & Rovainen, C. M. (1993) *J. Cereb. Blood Flow Metab.* **13,** 899–913.
47. Iadecola, C., Yang, G., Ebner, T. J. & Chen, G. (1997) *J. Neurophysiol.* **78,** 651–659.
48. Hamel, E. (2004) *Prog. Brain Res.* **145,** 171–178.
49. Iadecola, C. (2004) *Nat. Rev. Neurosci.* **5,** 347–360.
50. Harel, N., Lee, S. P., Nagaoka, T., Kim, D. S. & Kim, S. G. (2002) *J. Cereb. Blood Flow Metab.* **22,** 908–917.
51. Ogawa, S., Tank, D. W., Menon, R., Ellermann, J. M., Kim, S. G., Merkle, H. & Ugurbil, K. (1992) *Proc. Natl. Acad. Sci. USA* **89,** 5951–5955.
52. Shoham, D., Glaser, D. E., Arieli, A., Kenet, T., Wijnbergen, C., Toledo, Y., Hildesheim, R. & Grinvald, A. (1999) *Neuron* **24,** 791–802.
53. Simons, D. J. (1996) in *Cerebral Cortex*, eds. Jones, E. G. & Diamond, I. T. (Plenum, New York), Vol. 11, pp. 263–293.
54. Polley, D. B., Chen-Bee, C. H. & Frostig, R. D. (1999) *J. Neurophysiol.* **81,** 692–701.
55. Sheth, B. R., Moore, C. I. & Sur, M. (1998) *J. Neurophysiol.* **79,** 464–470.